Geophys. J. R. astr. Soc. (1981) **64**, 499–511

The effect of a second-order velocity discontinuity on elastic waves near their turning point

D. J. Doornbos★ *Vening Meinesz Laboratory, Budapestlaan 4, Postbus 80.021, 3508 TA Utrecht, The Netherlands*

Received 1980 May 12; in original form 1980 March 24

Summary. The rather abrupt changes in velocity gradient which have sometimes been proposed, notably in the upper mantle and near the base of the mantle, have an effect equivalent to that of one or more second-order discontinuities, where partial reflection occurs due to a change in curvature of the wavefront across these discontinuities. The effect is ignored in the classical WKBJ approximation to the wave functions, but it can be explicitly demonstrated by applying the extended WKBJ method (Langer's approximation) to a piecewise smooth layered model. For the purpose of this study it is convenient to represent the response of such a model by a generalized reflection coefficient. For a model of one or a system of several second-order discontinuities (approximating a change in velocity gradient over a finite depth interval), the reflection coefficient can be perhaps surprisingly large for long-period waves near their turning point. It is shown that this effect can significantly alter the amplitude decay of *SH* waves diffracted around the core, in models where a change in velocity gradient near the core–mantle boundary constitutes a low-velocity zone at the base of the mantle; such models have recently been proposed. With the same velocity gradients, the effect on *P* diffraction is less important. The results for *SH* diffraction in these models support the conclusion that a small amplitude decay must be explained by a velocity decrease with depth, i.e. a low-velocity zone at the base of the mantle.

1 Introduction

In an Earth model, second-order velocity discontinuities (i.e. discontinuities in the velocity gradient) may arise due to model parameterization, and their high-frequency effect has been demonstrated in applying geometrical ray theory (Julian & Anderson 1968). It is desirable to smooth this effect since it is an artefact of the model, and this is conveniently done in a WKBJ approximation (Chapman 1978). However, for some regions of the Earth, notably the upper mantle and the base of the mantle, it has sometimes been proposed that rather abrupt changes in velocity gradient occur in a relatively short depth interval. In these cases,

★Present address: NTNF/NORSAR, PO Box 51, 2007 Kjeller, Norway.

the model of one or more second-order discontinuities would still be a simplification but, in analogy to approximating rapid velocity changes by one or more first-order discontinuities, it would be a sensible approximation at relatively long wavelengths. It is the long-wavelength effect that we study in this paper. The effect is associated with a change in the curvature of a wavefront across a second-order discontinuity. This change is ignored in the classical WKBJ approximation, but it is described by the extended WKBJ method (the Langer approximation). Following Richards (1976) it is now widely appreciated that the extension of the WKBJ method is most important for long waves near their turning point, consequently the second-order discontinuity is expected to be most effective in the same circumstances. It was in fact the analysis of one such wave phenomenon, diffraction around the core, that has motivated the present study. Previous studies either implicitly ignored the effect (e.g. the extended WKBJ method in a smooth profile which is a version of the so-called full wave method), or the effect was taken into account without explicitly identifying it (e.g. the reflectivity method in an equivalent flat Earth model). These two different methods give very similar results in many cases, but a discrepancy has been noted for certain models and wave types, e.g. diffracted *SH* in models with a low-velocity zone at the base of the mantle.

In Section 2 we consider partial reflection at a second-order discontinuity, and demonstrate its significance in cases which are thought to be representative of some recently proposed models. A more complete analysis requires calculations in a layered model, and Section 3 summarizes the necessary theoretical framework. The basic point here is to extend the applicability of the conventional asymptotic propagator matrices (*cf.* Woodhouse 1978; Cormier 1980), but in many applications this can also be considered a means to generalize the concept of reflection coefficients (*cf.* Kennett 1974). Thus, by constructing generalized reflection coefficients for models including one or more second-order discontinuities near the core–mantle boundary, we are able to discuss in more detail the effect on diffraction around the core, in Section 4.

2 Reflection coefficients

In a vertically or radically inhomogenous medium, the Fourier transformed wavefield may be decomposed in surface harmonics, and propagation of displacement and stress components (neglecting gravity) may be expressed by

$$\partial_z \mathbf{D} = i\omega \mathbf{A} \mathbf{D}, \tag{1}$$

where, separately for *P–SV* and *SH*, **D** is the stress-displacement vector. Let a surface harmonic correspond to a fixed ray parameter p, then a horizontal wavenumber is $\omega q = \omega p/r$ in spherical geometry, $\omega q = \omega p$ in flat geometry. Then the zero-order approximation to the matrix **A** (e.g. Woodhouse 1978) is identical in the spherical and flat geometry (apart from a r^{-1} factor in the radial wave functions). Therefore, in the following we make no distinction between these two cases, unless explicitly stated. In an isotropic medium, the zero-order approximation implies decoupling of *P* and *SV* away from interfaces. Following Kennett, Kerry & Woodhouse (1978), the matrix **A** may be decomposed in eigenvalues and eigenvectors

$$\mathbf{A} = \mathbf{F} \Lambda \mathbf{F}^{-1},$$

where the eigenvectors of **A** are the columns of **F**, and these contain the vertical wave functions for *P* and *S*. If the wave functions are normalized, coefficients must be attached to them, and the matrix **F** also connects the wave coefficients (in the vector **B**) with the stress-displacement vector **D**

$$\mathbf{D} = \mathbf{F} \mathbf{B}. \tag{2}$$

This representation is in fact equivalent to that in terms of scalar potentials, by Richards (1974). Since **F** satisfies equation (1) it is called a matrizant, or fundamental matrix (e.g. Gilbert & Backus 1966). The form of **F** with up and downgoing waves used in this work is given in Appendix A.

At a solid–solid interface, **D** is continuous but **B** is not, and reflection/transmission coefficients may be obtained from elements of **F** evaluated on opposite sides of the interface. At a second-order discontinuity, the continuity condition for **D** is seen, from equation (2), to reduce to a continuity condition for the wavefield and its vertical derivative. This requires, at least in principle, coupling of up and downgoing waves (reflection), but no coupling between *P* and *SV*. The reflection/transmission coefficients for *P*, *SV* and *SH* are therefore given by similar expressions

$$\text{(upward reflection)}\quad \frac{A_u^+}{A_d^+} = \frac{U_d^+}{U_u^+}\,\frac{C_d^+ - C_d^-}{C_u^+ + C_d^-}, \tag{3}$$

$$\text{(downward transmission)}\quad \frac{A_d^-}{A_d^+} = \frac{U_d^+}{U_d^-}\left(1 - \frac{C_d^- - C_d^+}{C_u^+ + C_d^-}\right), \tag{4}$$

where superscript + and – denote the top and bottom side of the discontinuity, $U_{u/d}$ are up/downgoing wave functions, $A_{u/d}$ the up/downgoing wave coefficients, and $C_{u/d}$ the so-called generalized cosines which are related to vertical derivatives of the wave functions (Richards 1976). Similar expressions for downward reflection and upward transmission follow from symmetry considerations; for real angle of incidence, downward reflection equals upward reflection in absolute value.

In the WKBJ approximation of the wave functions: $C_u^+ = C_d^+ = C_u^- = C_d^- = \cos i$, where i is the angle of incidence, so in this approximation the second-order discontinuity has no effect. However, near a turning point the WKBJ solution is invalid and, following Chapman (1974) and Richards (1976), it has become almost common practice to extend the approximation by Langer's solution which, among other things, takes into account the difference in curvature of the wavefront on opposite sides of the interface. Fig. 1 illustrates the effect

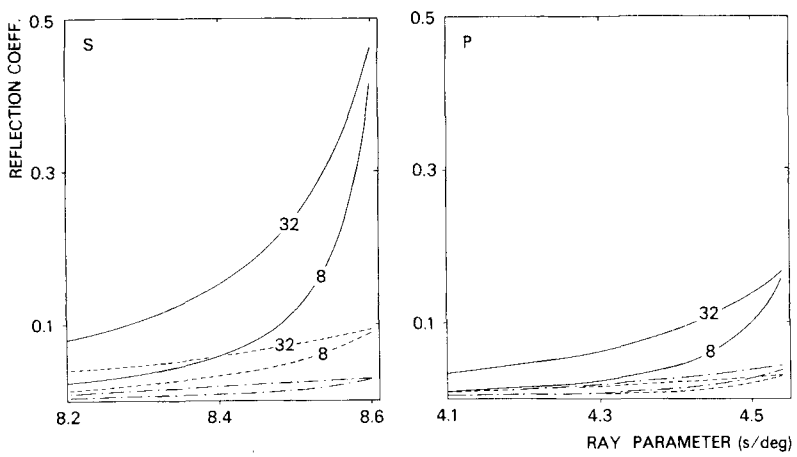

Figure 1. Reflection coefficients as a function of ray parameter for *P* and *S* waves at a period of 32 and 8 s. The interface is a second-order velocity discontinuity at radius 3560.7 km, $v_p = 13.661\ \mathrm{km\ s^{-1}}$, $v_s = 7.218\ \mathrm{km\ s^{-1}}$. ——— $= dv_p^+/dr = -0.001$, $dv_p^-/dr = 0.0019$, $dv_s^+/dr = -0.0004$, $dv_s^-/dr = 0.0019$. ---------- $= dv_p^+/dr = -0.001$, $dv_p^-/dr = -0.0019$, $dv_s^+/dr = -0.0004$, $dv_s^-/dr = -0.0019$. – – – – $= dv_p^+/dr = -0.001$, $dv_p^-/dr = 0$, $dv_s^+/dr = -0.0004$, $dv_s^-/dr = 0$. + and – refer to the top and bottom side of the interface.

by giving reflection coefficients for P and S waves, at a second-order discontinuity with velocities appropriate for the lower mantle near the core–mantle boundary. The changes in velocity gradients considered here encompass those of recently proposed models with and without low-velocity zones at the base of the mantle (e.g. Doornbos & Mondt 1979b; Mula & Müller 1980; Dziewonski and Anderson 1980). We make the following observations: (1) The reflection is a long-period phenomenon; at 1 s period the reflection is insignificant except for the trivial case that the turning point is practically at the interface, and it is not given in the figure. (2) A change to negative velocity gradient with depth (giving a low-velocity zone) is a stronger reflector than a change to positive gradient giving a high-velocity zone. (3) With the same change in gradient, S waves are reflected more strongly than P. Note here that because P and S velocities are different, the same gradient in spherical geometry implies a different gradient in the equivalent flat geometry.

3 A layered model

Certain model restrictions are implicit in obtaining results as described in the previous section. First, Langer's solution requires a classical turning point and hence would preclude zones with sufficiently negative velocity gradient with depth (i.e. in flat geometry $dv/dz > 0$ if z is positive upward; in spherical geometry $dv/dr > v/r$). The restriction can be removed by considering that, in flat geometry, the choice of up or downgoing wave is dictated by the choice of sign of z coordinate. Simply reversing the z coordinate, or what amounts to the same and is also applicable in spherical geometry, reversing the computed vertical phase $\omega\tau$ with τ the usual 'tau function' (Bessonova *et al.* 1976), leads to solutions with up and downgoing wave functions, and their associated generalized cosines, interchanged. The validity of this result in spherical geometry can also be demonstrated by applying an earth-flattening transformation. As a final step then, we have to undo this interchange before computing reflection coefficients.

The second point is that single reflection in the model of two half spaces is often an over-simplified concept; multiple reflection must be taken into account especially for waves near their turning point. In its simplest form this could be done by replacing the downgoing wave and its generalized cosine in equations (3) and (4), by a standing wave (Cormier & Richards 1977). However, a more general layered model would also account for the interaction with nearby discontinuities, and it may be used to approximate a pseudo second-order discontinuity characterized by a change in velocity gradient over a finite depth interval. Layered models have been, and still are being, treated extensively in the literature. A recent review is by Kennett & Kerry (1979). In practical applications, the reflectivity method of Fuchs & Müller (1971) has been widely used, and in some recent work Langer's approximation is used to extend the method (Woodhouse 1978; Cormier 1980). The formal structure of the solution is, however, independent of the particular type of wave functions, and only an outline of the procedure will be given here. For indexing of layers and interfaces, we refer to Fig. 2.

From the fundamental matrices for the individual layers, and the continuity condition for stress-displacement across interfaces, propagator matrices (Gilbert and Backus 1966) are constructed which relate stress-displacement at the top and bottom interface

$$\mathbf{D}_0 = \mathbf{P}_{0,N}\mathbf{D}_N - \mathbf{P}_{0,s}[\mathbf{D}_s]^+_-, \tag{5}$$

where $\mathbf{P}_{0,N}$, $\mathbf{P}_{0,s}$ are propagator products between interfaces 0–N and 0–s, respectively. In the P–SV case, these products of layer matrices generally couple P and SV propagation, but if the interfaces are second-order discontinuities, P and SV remain uncoupled and the propagator matrix can be partitioned accordingly. The second term in equation (5) includes

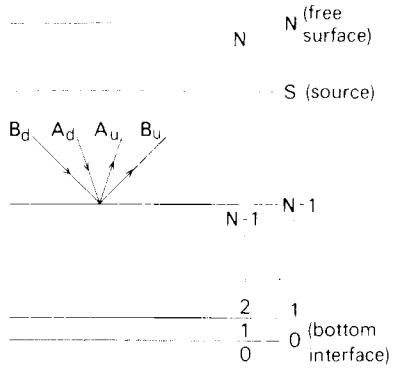

Figure 2. Indexing of layers and interfaces. $A_{u/d}$, $B_{u/d}$ are up/downgoing wave coefficients for P and S in layer N.

a source effect by representing it as a dislocation in displacement and stress across a level z_s, a procedure introduced by Hudson (1969). The relation (5) was given by Kennett & Kerry (1979) in a slightly different form. The solution for $\mathbf{D}_N$ (or at any other level) may now be obtained by applying boundary conditions, usually to $\mathbf{D}_0$ and $\mathbf{D}_N$. One usually applies the stress-free surface condition to $\mathbf{D}_N$, and $\mathbf{D}_0$ is related to conditions of downward radiation, or exponential decay, of the wavefield below z_0. Different versions of the solution are given, e.g. by Kennett & Kerry (1979) and Cormier (1980). In view of the application in the next section, it is also of interest to include the case of a solid–liquid interface. A summary of formulae is given in Appendix B.

The solutions in the form of equation (B1) and (B2) include the effect of second-order discontinuities if these are taken to coincide with interfaces of the model. However, following Kennett & Kerry (1979) it may be useful to explicitly identify the reflection coefficients from a stack of layers (including second-order discontinuities). Earlier applications to the problem of diffraction around the core are from Phinney & Alexander (1966) and Chapman & Phinney (1972). If we consider reflection from the layer stack 0, . . . , N–1 (Fig. 2), the procedure differs from the foregoing mainly in that boundary conditions at the top of layer N are replaced by radiation conditions in layer N. The resulting reflection coefficients for SH and P–SV are given by equations (B6) and (B7) of the Appendix. In this case, excitation by a source must be contained in the downgoing wave coefficients A_d, B_d. In Appendix C these wave coefficients are expressed in terms of the source dislocation vector $[\mathbf{D}_s]^+_-$; alternative expressions may be found in Kennett & Kerry (1979).

When the reflected wavefield is represented in terms of scalar potentials we have, e.g. for P at level z:

$$\phi(z) = A_u U_u(z)$$

and equations (B7), (C1) and (C3) may be used to find

$$\phi(z) = RK(z_s)\, U_u(z_s)\, U_u(z), \tag{6}$$

where R is the reflection coefficient A_u/A_d, and $K(z_s)\, U_u(z_s)$ is the excitation function. This is the form of Richards (1973) which has been used in previous applications of 'full wave theory' (e.g. Mondt 1977; Cormier & Richards 1977; Choy 1977; Doornbos & Mondt 1979b). Finally, it may be recalled that all solutions discussed here correspond to one surface harmonic, so the various factors in equations like (6) depend on ω and p although this has not been brought out in the notation. These solutions are to be substituted in inverse transformations,

a rather complete account of which has been given by Chapman (1978). In the applications of full wave theory, the inverse transformation involves an integration in the complex ray parameter plane, following Richards (1973).

4 Diffraction around the core

It is of interest to consider a second-order discontinuity in the neighbourhood of a first-order discontinuity, first because such models actually have been proposed (e.g. Dziewonski & Anderson 1980), and second because first-order discontinuities have associated with them diffracted waves, and these waves satisfy the requirements for second-order discontinuities to be effective. One of the clearest examples of such a model, with one of the most observed and studied diffraction patterns, is the region near the core–mantle boundary. Observations bearing on this region have sometimes been controversial, as have the models inferred from them (e.g. Doornbos & Mondt 1979b; Okal & Geller 1979; Mula & Müller 1980). Seismological effects of various proposed anomalies in the core–mantle boundary region have been discussed by Doornbos & Mondt (1979a); the effect of second-order discontinuities was not considered. It is the purpose of this section to demonstrate this effect for recently proposed models, by presenting results for the diffraction pattern as it is usually analysed, i.e. in the form of phase velocity or $dT/d\Delta$, and exponential decay per unit of epicentral distance. To compute these parameters, equation (6) has been used in an inverse ray parameter transformation (*cf.* equation 9 of Doornbos & Mondt 1979b).

We have obtained results for perturbations of two reference models, PEM-C of Dziewonski, Hales & Lapwood (1975) and PREM of Dziewonski & Anderson (1980); the effect was similar in these two cases. Of the results obtained, we present those which are thought to be representative of recently proposed models, and which are illustrative with regard to the effect discussed here. It was observed in Section 2 that the effect is more significant for *S* waves, at long periods, and in models having a velocity decrease below the second-order discontinuity. These inferences are confirmed here, and these cases will be given more attention than others. Another important model parameter is the thickness of transition zone; a very thin zone might be 'transparent' to long-period waves, in a very thick zone diffraction may not be much affected by the second-order discontinuity. The models we discuss here have a 75 km thick transition zone; they are shown in Fig. 3. Observational parameters of long-period diffracted waves have been obtained usually from records roughly in the epicentral distance range 95°–135°. We compute $dT/d\Delta$ and decay γ as a function of frequency, over the same distance range. Results are shown in Figs 4 and 5, and we will discuss some of the main features.

It is now well established that for subcritical velocity gradients (i.e. $dv/dr < v/r$), the decay γ is smaller if the velocity is more decreasing toward the core–mantle boundary. Ignoring the effect of a second-order discontinuity, one would expect γ to be minimal for velocities near the critical gradient. If the velocity decreases more with depth, i.e. has a supercritical gradient, no turning point exists in the low-velocity zone and the ray-geometrical shadow boundary shifts backward to shorter distances. In that case the effect of a second-order discontinuity will be to create the conditions for a waveguide in the low-velocity zone, and the decay may, at least at some commonly observed frequencies, be very similar to decay with subcritical gradients but without a second-order discontinuity. In Fig. 4 this is illustrated for *SH* by comparing models (2) (solid line) and (4) (dashed line). Including the effect of the second-order discontinuity in model (2) (dashed line) increases the *SH* decay in the distance range considered here. This explains a discrepancy between *SH* results by Fuchs & Müller's (1971) reflectivity method and by the full wave method (Mondt & Pootjes 1980), while for *P* diffraction no such discrepancy was observed (Mula & Müller, private communication). The

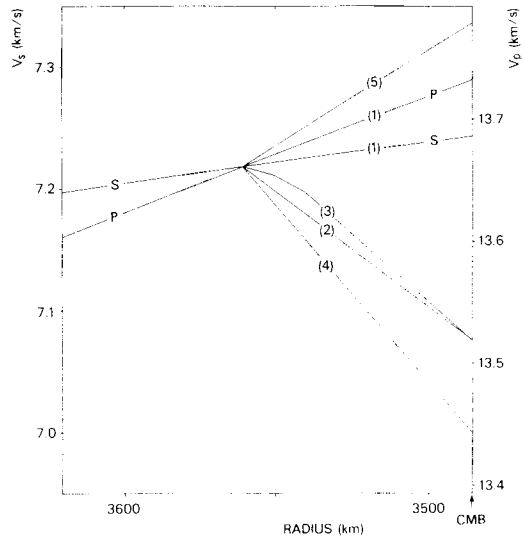

Figure 3. Velocity models of the lower mantle. The reference model (PEM-C) which is labelled (1) for both P and S, is perturbed to produce second-order discontinuities. The velocity perturbations have been chosen to give for P and S the same velocity gradients in the transition zone.

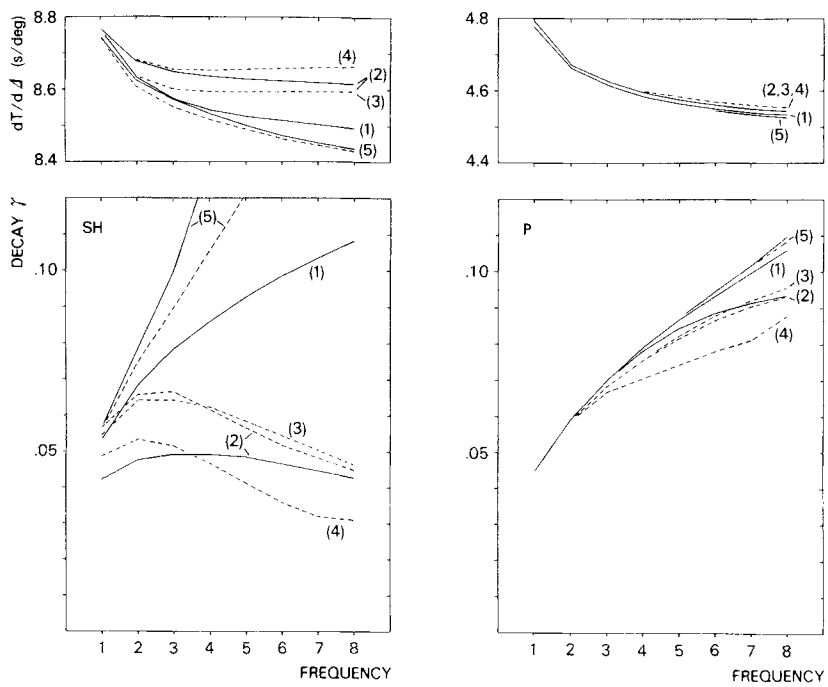

Figure 4. Decay spectra and $dT/d\Delta$ for P and SH in the distance range 95°–135°, for the models in Fig. 3. γ measures decay per degree of epicentral distance, and frequency points 1, . . . , 8 correspond to 0.015625, . . . , 0.125 Hz in steps of 0.015625. Results are labelled corresponding to the models. ——— ; Effect of second-order discontinuity ignored; ---------- : effect included.

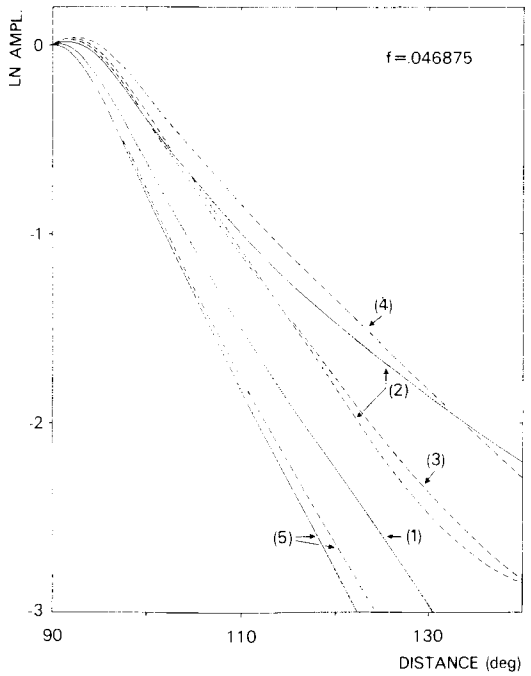

Figure 5. Amplitude decay of *SH* in the distance range 90°–140°, at the frequency 0.046875, for the models in Fig. 3. Results are labelled corresponding to the models. ——— : Effect of second-order discontinuity ignored; ---------- : effect included.

increased decay may be ascribed to partial reflection off the top of the transition zone. At larger distances the wave-guide effect becomes more important and the decay is smaller, but observations are not usually made in that distance range. The change of amplitude decay with distance is shown in Fig. 5, for one typical long period (near 20 s). By comparing models (2) and (3) (dashed line) in Figs 4 and 5, it is also shown that the long-period effect is rather similar for a 'pseudo' second-order discontinuity, where the change in velocity gradient occurs over a finite depth interval which is short compared to the wavelength.

The effect of increased decay is obtained only in low-velocity zones; in high-velocity zones on the contrary, the effect is to decrease the decay (*cf.* model 5), although it remains always higher than for the standard model. In all these cases there is also an effect on $dT/d\Delta$ (Fig. 4); in general, higher decay corresponds to lower $dT/d\Delta$ and vice versa. This effect would be difficult to identify, however, since $dT/d\Delta$ also depends strongly on the absolute velocity values, not just the gradients. For example, the difference in $dT/d\Delta$ for diffracted *SH* in the PEM-C and PREM models is about 0.1 s deg^{-1}.

Finally, Fig. 4 shows that for recently proposed models, the effect on *P* diffraction is of lower importance. It may become important for zones with very low velocities (*cf.* model 4), but such drastic changes have not been proposed lately. $dT/d\Delta$ for long-period *P* is virtually the same in all these models.

5 Conclusions

Partial reflection at a second-order, or pseudo second-order velocity discontinuity may be a significant phenomenon for long-period waves near their turning point. In an Earth model it is more significant for *S* than for *P* waves due to the lower *S* velocities, and it is more significant if the model includes a low-velocity zone in which the velocity decreases with

depth. The effect is ignored in the classical WKBJ method, but not in the extended method which takes into account difference in curvature of wave front on opposite sides of the discontinuity. Calculations in a layered model are necessary to demonstrate the effect, and they explain certain differences noted between results for *SH* waves with the 'classical' reflectivity method (which takes the effect into account but does not explicitly identify it) and a version of the so-called full wave method which ignores layering; the restriction to subcritical velocity gradients (i.e. $dv/dr < v/r$) in that version can also be removed.

The interpretation of long-period *SH* waves diffracted around the core has been the subject of some discussion in recent years, and it may be of interest to summarize the most important effects from an observational point of view, of proposed (pseudo) second-order velocity discontinuities near the core–mantle boundary: If the change in velocity gradient constitutes a low-velocity zone in which the gradient is subcritical, the effect on *SH* is to increase the amplitude decay in the usually observed distance range (~95°–135°). If the gradient becomes supercritical, the wave-guide effect of the low-velocity layer may be sufficient to give low-decay values, comparable to what is obtained for a subcritical low-velocity zone with the second-order discontinuity absent (or ignored). These results together with actually observed low-decay values, continue to stress the concept of a low-velocity zone at the base of the mantle. The effect on long-period diffracted *P* waves is less important, at least for velocity gradients which are in the range of recently proposed models.

Acknowledgments

I thank Dr Mondt for discussions on the diffraction problem. This paper is NORSAR contribution No. 275.

References

Abo-Zena, A., 1979. Dispersion function computations for unlimited frequency values, *Geophys. J. R. astr. Soc.*, **58**, 91–105.

Bessonova, E. N., Fishman, V. M., Shnirman, M. G., Sitnikova, G. A. & Johnson, L. R., 1976. The tau method for inversion of travel times – II. Earthquake data, *Geophys. J. R. astr. Soc.*, **46**, 87–108.

Chapman, C. H., 1974. The turning point of elastodynamic waves, *Geophys. J. R. astr. Soc.*, **39**, 613–622.

Chapman, C. H., 1978. A new method for computing synthetic seismograms, *Geophys. J. R. astr. Soc.*, **54**, 481–518.

Chapman, C. H. & Phinney, R. A., 1972. Diffracted seismic signals and their numerical solution, in *Meth. Comput. Phys.*, **12**, 165–230, ed. Bolt, B. A.

Choy, G. L., 1977. Theoretical seismograms of core phases calculated by frequency-dependent full wave theory, and their interpretation, *Geophys. J. R. astr. Soc.*, **51**, 275–312.

Cormier, V. F., 1980. The synthesis of complete seismograms in an Earth model specified by radially inhomogeneous layers, *Bull. seism. Soc. Am.*, in press.

Cormier, V. F. & Richards, P. G., 1977. Full wave theory applied to a discontinuous velocity increase: The inner core boundary, *J. Geophys.*, **43**, 3–31.

Doornbos, D. J. & Mondt, J. C., 1979a. Attenuation of *P* and *S* waves diffracted around the core, *Geophys. J. R. astr. Soc.*, **57**, 353–379.

Doornbos, D. J. & Mondt, J. C., 1979b. *P* and *S* waves diffracted around the core and the velocity structure at the base of the mantle, *Geophys. J. R. astr. Soc.*, **57**, 381–395.

Dziewonski, A. M., Hales, A. L. & Lapwood, E. R., 1975. Parametrically simple Earth models consistent with geophysical data, *Phys. Earth planet. Interiors*, **10**, 12–48.

Dzeiwonski, A. M. & Anderson, D. L., 1980. A proposal for an interim reference Earth model, *Phys. Earth planet. Interiors*, in press.

Fuchs, K. & Muller, G., 1971. Computation of synthetic seismograms with the reflectivity method and comparison with observations, *Geophys. J. R. astr. Soc.*, **23**, 417–433.

Gilbert, F. & Backus, G. E., 1966. Propagator matrices in elastic wave and vibration problems, *Geophysics*, **31**, 326–332.

Hudson, J. A., 1969. A quantitative evaluation of seismic signals at teleseismic distances – I. Radiation from point sources, *Geophys. J. R. astr. Soc.*, **18**, 233–249.

Julian, B. R. & Anderson, D. L., 1968. Travel times, apparent velocities and amplitudes of body waves, *Bull. seism. Soc. Am.*, **58**, 339–366.

Kennet, B. L. N., 1974. Reflections, rays and reverberations, *Bull. seism. Soc. Am.*, **65**, 1643–1651.

Kennett, B. L. N., Kerry, N. J. & Woodhouse, J. H., 1978. Symmetries in the reflection and transmission of elastic waves, *Geophys. J. R. astr. Soc.*, **52**, 215–230.

Kennett, B. L. N. & Kerry, N. J., 1979. Seismic waves in a stratified half space, *Geophys. J. R. astr. Soc.*, **57**, 557–583.

Menke, W., 1979. Comment on 'Dispersion function computations for unlimited frequency values' by Anas Abo-Zena, *Geophys. J. R. astr. Soc.*, **59**, 315–323.

Mondt, J. C., 1977. SH waves: theory and observations for epicentral distances greater than 90 degrees, *Phys. Earth planet. Interiors*, **15**, 46–59.

Mondt, J. C. & Pootjes, H. J., 1980. A comparison of the reflectivity method and full wave theory, as applied to the SH diffraction around the core, *Pure appl. Geophys.*, in press.

Mula, A. H. & Muller, G., 1980. Ray parameters of diffracted long period P and S waves and the velocities at the base of the mantle, *Pure appl. Geophys.*, in press.

Okal, E. A. & Geller, R. J., 1979. Shear-wave velocity at the base of the mantle from profiles of diffracted SH waves, *Bull. seism. Soc. Am.*, **69**, 1039–1053.

Phinney, R. A. & Alexander, S. S., 1966. P wave diffraction theory and the structure of the core–mantle boundary, *J. geophys. Res.*, **71**, 5959–5975.

Richards, P. G., 1973. Calculation of body waves for caustics and tunnelling in core phases, *Geophys. J. R. astr. Soc.*, **35**, 243–264.

Richards, P. G., 1974. Weakly coupled potentials for high-frequency elastic waves in continuously stratified media, *Bull. seism. Soc. Am.*, **64**, 1575–1588.

Richards, P. G., 1976. On the adequacy of plane-wave reflection/transmission coefficients in the analysis of seismic body waves, *Bull. seism. Soc. Am.*, **66**, 701–717.

Schwab, F. A. & Knopoff, L., 1972. Fast surface wave and free mode computations, in *Math. Comput. Phys.*, **11**, 87–180, ed. Bolt, B. A.

Woodhouse, J. H., 1978. Asymptotic results for elastodynamic propagator matrices in plane stratified and spherically stratified Earth models, *Geophys. J. R. astr. Soc.*, **54**, 263–281.

Appendix A: Fundamental matrices

The forms given by different authors are sometimes different due to different arrangement and normalization of stress-displacement and wave coefficients. Therefore, we give here the forms as used in the present work. The wave coefficients we used, $A_{u/d}$ for up/downgoing P, $B_{u/d}$ for up/downgoing S waves, are related to the scalar potentials in Richards' (1974) representation of displacement. At a fixed ray parameter p and omitting the horizontal phase factor $\exp(i\omega px)$ in flat geometry, or $\exp(i\omega p\theta)$ in spherical geometry:

$$\begin{aligned} \phi &= (A_u U_u + A_d U_d), && (P \text{ waves}) \\ \psi &= \frac{1}{-i\omega p}(B_u V_u + B_d V_d), && (\text{SV and SH waves}) \end{aligned} \tag{A1}$$

where $U_{u/d}$, $V_{u/d}$ are up/downgoing wave functions for P and S, respectively.

The representation, in the form of equation (2) of the main text, becomes for SH:

$$\begin{pmatrix} u_y \\ \tau_{zy}/i\omega \end{pmatrix} = \mu^{-1/2} \begin{pmatrix} 1 & 1 \\ \mu D_u/\beta & -\mu D_d/\beta \end{pmatrix} \begin{pmatrix} V_u & 0 \\ 0 & V_d \end{pmatrix} \begin{pmatrix} B_u \\ B_d \end{pmatrix}, \tag{A2}$$

where u_y, τ_{zy} are displacement and stress components, μ is rigidity and $D_{u/d}$ are the generalized cosines for S:

$$\frac{D_{u/d}}{\beta} = \pm(\partial_z V_{u/d})/(i\omega V_{u/d}).$$

In the notation of equation (2), the wave coefficient vector **B** has here the elements B_u, B_d, and the matrix **F** has been decomposed to display more explicitly the role of the up and downgoing wave functions V_u, V_d.

Similarly, for *P–SV*:

$$\begin{pmatrix} u_x \\ u_z \\ \tau_{zx}/i\omega \\ \tau_{zz}/i\omega \end{pmatrix} = i\omega\rho^{-1/2} \begin{pmatrix} q & q & D_u/\beta & -D_d/\beta \\ C_u/\alpha & -C_d/\alpha & -q & -q \\ 2\mu q C_u/\alpha & -2\mu q C_d/\alpha & -\mu\nu & -\mu\nu \\ -\mu\nu & -\mu\nu & -2\mu q D_u/\beta & 2\mu q D_d/\beta \end{pmatrix} \begin{pmatrix} U_u & 0 & 0 & 0 \\ 0 & U_d & 0 & 0 \\ 0 & 0 & V_u & 0 \\ 0 & 0 & 0 & V_d \end{pmatrix} \begin{pmatrix} A_u \\ A_d \\ B_u \\ B_d \end{pmatrix}, \quad \text{(A3)}$$

where ρ is density, $\upsilon = 2q^2 - 1/\beta^2$, $q = p$ in flat geometry, $q = p/r$ in spherical geometry, and $C_{u/d}$ are the generalized cosines for *P*.

For a liquid, the fundamental matrix reduces to a 2 x 2 matrix.

Although the notation for stress-displacement components in equations (A2) and (A3) is that conventionally taken in a Cartesian coordinate system, the asymptotic relations hold more generally, e.g. in cylindrical and spherical coordinates.

Appendix B: Response of a layered model

For the free surface displacement response we follow the representation of Cormier (1980), with minor modifications. The meaning of the propagator matrices $\mathbf{P}_{0,N}$ and $\mathbf{P}_{N,s} = \mathbf{P}_{s,N}^{-1}$, the fundamental matrix below the bottom interface $\mathbf{F}_0$, and the source vector $[\mathbf{D}_s]_-^+$, is as in Sections 2 and 3.

For *SH*:

$$u_y = \mathbf{G}_{0,N}^T \mathbf{P}_{N,s} [\mathbf{D}_s]_-^+ \Big/ \mathbf{G}_{0,N}^T \begin{pmatrix} 1 \\ 0 \end{pmatrix}, \quad \text{(B1)}$$

$$\mathbf{G}_{0,N}^T = \mathbf{E}^T \mathbf{P}_{0,N}.$$

For *P–SV*

$$\begin{pmatrix} u_x \\ \\ u_y \end{pmatrix} = \begin{pmatrix} 0 & -1 & 0 & 0 \\ & & & \\ 1 & 0 & 0 & 0 \end{pmatrix} \mathbf{G}_{0,N} \mathbf{P}_{N,s} [\mathbf{D}_s]_-^+ \Big/ (1,0,0,0)\, \mathbf{G}_{0,N} \begin{pmatrix} 0 \\ 1 \\ 0 \\ 0 \end{pmatrix}, \quad \text{(B2)}$$

$$\mathbf{G}_{0,N} = \mathbf{P}_{0,N}^T (\mathbf{E}_1 \mathbf{E}_2^T - \mathbf{E}_2 \mathbf{E}_1^T)\, \mathbf{P}_{0,N}$$

where, with a radiation condition below the bottom interface

$$\mathbf{E}_{SH}^T = (1,0)\, \mathbf{F}_0^{-1}(z_0), \qquad \begin{pmatrix} \mathbf{E}_1^T \\ \\ \mathbf{E}_2^T \end{pmatrix}_{PSV} = \begin{pmatrix} 1 & 0 & 0 & 0 \\ & & & \\ 0 & 0 & 1 & 0 \end{pmatrix} \mathbf{F}_0^{-1}(z_0). \quad \text{(B3)}$$

With an exponential decay condition below the bottom interface:

$$\mathbf{E}_{SH}^{T} = (1, -1)\,\mathbf{F}_0^{-1}(z_0), \qquad \begin{pmatrix} \mathbf{E}_1^{T} \\ \\ \mathbf{E}_2^{T} \end{pmatrix}_{PSV} = \begin{pmatrix} 1 & -1 & 0 & 0 \\ & & & \\ 0 & 0 & 1 & -1 \end{pmatrix} \mathbf{F}_0^{-1}(z_0). \tag{B4}$$

For a solid–liquid bottom interface:

$$\mathbf{E}_{SH}^{T} = (0, 1),$$

and for *P–SV* with, e.g. a radiation condition

$$\begin{pmatrix} \mathbf{E}_1^{T} \\ \\ \mathbf{E}_2^{T} \end{pmatrix}_{PSV} = \begin{pmatrix} (1,0)\,\mathbf{F}_0^{-1} \begin{pmatrix} 0 & 1 & 0 & 0 \\ & & & \\ 0 & 0 & 0 & 1 \end{pmatrix} \\ \hline 0 \quad 0 \quad 1 \quad 0 \end{pmatrix}. \tag{B5}$$

Here $\mathbf{F}_0$ is the 2 x 2 fundamental matrix of the liquid.

The specific form of $\mathbf{E}^{T}$, $\mathbf{E}_1^{T}$, $\mathbf{E}_2^{T}$ reflects our choice of up and downgoing wave functions in the fundamental matrix $\mathbf{F}$, equations (A2), (A3). A different choice would give different combinations of rows of $\mathbf{F}_0^{-1}$ (*cf.* Cormier 1980). The propagation of minors of $\mathbf{F}^{-1}$, i.e. $\mathbf{E}_1\mathbf{E}_2^{T} - \mathbf{E}_2\mathbf{E}_1^{T}$, has been discussed by Cormier and others, e.g. Menke (1979), Abo Zena (1979), Schwab & Knopoff (1972).

To obtain reflection coefficients from the layer stack $0, \ldots, N-1$ (Fig. 2), the stress displacement vector at the interface $N-1$ must be related to a radiation condition in layer N above this interface. This relation is given through the fundamental matrix of this layer. Apart from this additional matrix multiplication, the structure of the solution is rather similar to that of the displacement response. The reflection coefficients are given as ratios of wave coefficients. For *SH*

$$(B_u/B_{dN}) = -\mathbf{G}_{0,N-1}^{T}\mathbf{F}_N(z_{N-1}) \begin{pmatrix} 0 \\ \\ 1 \end{pmatrix} \Big/ \mathbf{G}_{0,N-1}^{T}\mathbf{F}_N(z_{N-1}) \begin{pmatrix} 1 \\ \\ 0 \end{pmatrix} \tag{B6}$$

For *P–SV*

$$\begin{pmatrix} A_u/A_d, A_u/B_d \\ B_u/A_d, B_u/B_d \end{pmatrix}_N = - \frac{\begin{pmatrix} 0 & 0 & -1 & 0 \\ 1 & 0 & 0 & 0 \end{pmatrix} \mathbf{F}_N^{T}(z_{N-1})\mathbf{G}_{0,N-1}\mathbf{F}_N(z_{N-1}) \begin{pmatrix} 0 & 0 \\ 1 & 0 \\ 0 & 0 \\ 0 & 1 \end{pmatrix}}{(1 \quad 0 \quad 0 \quad 0)\ \mathbf{F}_N^{T}(z_{N-1})\mathbf{G}_{0,N-1}\mathbf{F}_N(z_{N-1}) \begin{pmatrix} 0 \\ 0 \\ 1 \\ 0 \end{pmatrix}}$$

with $\mathbf{G}^{T}$, $\mathbf{G}$ defined in equations (B1) and (B2).

Appendix C: Excitation functions for the wave coefficients

Applying equation (2) on opposite sides of the source level we have

$$[\mathbf{D}_s]^+_- = \mathbf{F}(z_s)[\mathbf{B}_s]^+_-,$$

where all functions are evaluated at the source level, and $[\mathbf{B}_s]^+_-$ denotes the jump in wave coefficients across this level. Applying the radiation condition

$$A_d^+ = A_u^- = B_d^+ = B_u^- = 0,$$

(no 'inward' radiation) we obtain

$$\mathbf{B}_s^{\pm} = \mathbf{F}^{-1}(z_s)[\mathbf{D}_s]^+_-,$$

where, for SH

$$\mathbf{B}_s^{\pm\,\mathrm{T}} = (B_u^+, -B_d^-)_s$$

for *P–SV*

$$\mathbf{B}_s^{\pm\,\mathrm{T}} = (A_u^+, -A_d^-, B_u^+, -B_d^-)_s.$$

The inverse fundamental matrix may be decomposed:

$$\mathbf{F}^{-1} = \mathbf{WK},$$

where $\mathbf{W}$ is diagonal with elements $\sim\alpha/\{U_{u/d}(C_u + C_d)\}$ and $\sim\beta/\{V_{u/d}(D_u + D_d)\}$. For asymptotic functions:

$$\alpha/\{U_{u/d}(C_u + C_d)\} = \frac{\pi}{4}\omega U_{d/u},$$

where we have normalized the wave functions as in equation (23) of Richards (1976). Then we have the excitation coefficients

$$\mathbf{B}_s^{\pm} = \mathbf{W}(z_s)\,\mathbf{K}(z_s)[\mathbf{D}_s]^+_-,$$

with, for *SH*

$$\mathbf{W}(z_s)\,\mathbf{K}(z_s) = \frac{\pi}{4}\omega\mu^{-1/2}\begin{pmatrix} V_d & 0 \\ 0 & V_u \end{pmatrix}_{z_s}\begin{pmatrix} \mu D_d/\beta & 1 \\ \mu D_u/\beta & -1 \end{pmatrix}_{z_s}. \tag{C2}$$

For *P–SV*

$$\mathbf{W}(z_s)\,\mathbf{K}(z_s) = -i\frac{\pi}{4}\rho^{-1/2}\begin{pmatrix} U_d & 0 & 0 & 0 \\ 0 & U_u & 0 & 0 \\ 0 & 0 & V_d & 0 \\ 0 & 0 & 0 & V_u \end{pmatrix}_{z_s}$$

$$\begin{pmatrix} 2\mu q C_d/\alpha & -\mu\nu & q & C_d/\alpha \\ 2\mu q C_u/\alpha & \mu\nu & -q & C_u/\alpha \\ -\mu\nu & -2\mu q D_d/\beta & D_d/\beta & -q \\ \mu\nu & -2\mu q D_u/\beta & D_u/\beta & q \end{pmatrix}_{z_s}. \tag{C3}$$

The various quantities appearing in these expressions have been defined in Appendix A.